RMIT University

Split-ring resonator for the slotted waveguide antenna and tuneable BST varactor

March, 2012

Prof. Kamran Ghorbani
School of Electrical & Computer Engineering, RMIT University

Report Documentation Page

Form Approved
OMB No. 0704-0188

1. REPORT DATE	2. REPORT TYPE	3. DATES COVERED
24 APR 2012	**Final**	**14-04-2011 to 13-04-2012**

4. TITLE AND SUBTITLE
Tunable Metamaterials for Antenna Applications

5a. CONTRACT NUMBER
FA23861114044

5b. GRANT NUMBER

5c. PROGRAM ELEMENT NUMBER

6. AUTHOR(S)
Kamran Ghorbani

5d. PROJECT NUMBER

5e. TASK NUMBER

5f. WORK UNIT NUMBER

7. PERFORMING ORGANIZATION NAME(S) AND ADDRESS(ES)
RMIT University,GPO BOX 2476,Melbourne VIC 3000,Australia,AU,3000

8. PERFORMING ORGANIZATION REPORT NUMBER
N/A

9. SPONSORING/MONITORING AGENCY NAME(S) AND ADDRESS(ES)
AOARD, UNIT 45002, APO, AP, 96338-5002

10. SPONSOR/MONITOR'S ACRONYM(S)
AOARD

11. SPONSOR/MONITOR'S REPORT NUMBER(S)
AOARD-114044

12. DISTRIBUTION/AVAILABILITY STATEMENT
Approved for public release; distribution unlimited

13. SUPPLEMENTARY NOTES

14. ABSTRACT
The increasing use of carbon fibre reinforced polymer CFRP in modern military aircraft together with the desire for a conformal load-bearing antenna structure, has since inspired the slotted waveguide antenna stiffened structure (SWASS) concept. Conventional hat stiffened or blade stiffened aircraft panels fabricated in CFRP coincidentally exhibit internal dimensions that are typical of common military waveguide bands. By machining resonant slots at half-wavelength intervals in the outer skin of the stiffened panel, a SWA may be integrated into the aircraft structure to achieve potential weight and drag improvements over conventional aircraft antennas. These slots may be filled with a low-loss dielectric to retain the aerodynamic performance of the panel or with a high dielectric to reduce their physical dimensions. Regardless, the structural impact of the slot is a significant concern for the SWASS concept.

15. SUBJECT TERMS
meta materials, Antennas

16. SECURITY CLASSIFICATION OF:			17. LIMITATION OF ABSTRACT	18. NUMBER OF PAGES	19a. NAME OF RESPONSIBLE PERSON
a. REPORT	b. ABSTRACT	c. THIS PAGE			
unclassified	**unclassified**	**unclassified**	**Same as Report (SAR)**	**11**	

1 Introduction

The increasing use of carbon fibre reinforced polymer CFRP in modern military aircraft together with the desire for a conformal load-bearing antenna structure, has since inspired the slotted waveguide antenna stiffened structure (SWASS) concept [1]. Conventional hat stiffened or blade stiffened aircraft panels fabricated in CFRP coincidentally exhibit internal dimensions that are typical of common military waveguide bands. By machining resonant slots at half-wavelength intervals in the outer skin of the stiffened panel, a SWA may be integrated into the aircraft structure to achieve potential weight and drag improvements over conventional aircraft antennas. These slots may be filled with a low-loss dielectric to retain the aerodynamic performance of the panel or with a high dielectric to reduce their physical dimensions. Regardless, the structural impact of the slot is a significant concern for the SWASS concept [2].

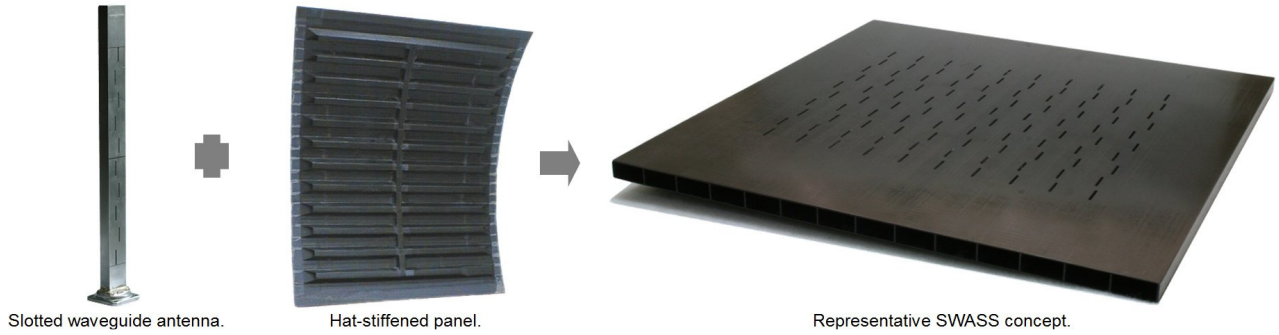

Figure 1.1: The SWASS Concept.

This report is divided into two sections: Section 2 validates the metamaterial inspired approach to SWASS that was described in Report AOARD104039. Section 3 describes the manufacture of BST varactors using the new sputterer at RMIT university.

2 Experimental validation of the SRR loaded sub-wavelength slot

To validate the numerical simulations of the SRR loaded SWA design cell described in Report AOARD104039, a single SRR was fabricated with the dimensions summarised in Table 2.1.

Table 2.1: SRR dimensions for fabrication on Rogers RT/duroid© 5880 (0.508 mm thick) substrate with 0.5 oz. copper metallisation.

Ring width	0.80 mm
Ring *x* dimension	9.44 mm
Ring *y* dimension	3.00 mm
Ring split dimension	0.1 mm

The SRR sample was adhered to a small piece of Rohacell HF foam using commercial cyanoacrylate and positioned in the WR-137 waveguide test fixture as illustrated in Figure 2.3. To ensure the outer edge of the SRR was located 0.5 mm beneath the waveguide broad

wall, the substrate was mounted slightly proud of the waveguide fixture. When the cover plate (with 0.35 λ_0 slot) was installed, the SRR sample was pressed into the correct position.

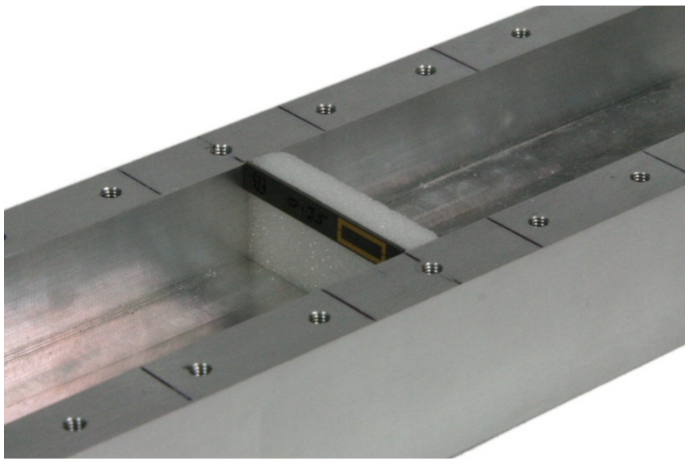

Figure 2.1: WR-137 test fixture (cover plate removed) with SRR element.

The Agilent PNA-X series vector network analyser was first calibrated according to the Thru-Reflect-Line procedure using WR-137 waveguide standards. The S-parameters of the SRR loaded 0.35 λ_0 slot were then measured. The simulated and measured S-parameter results are compared in Figure 2.2.

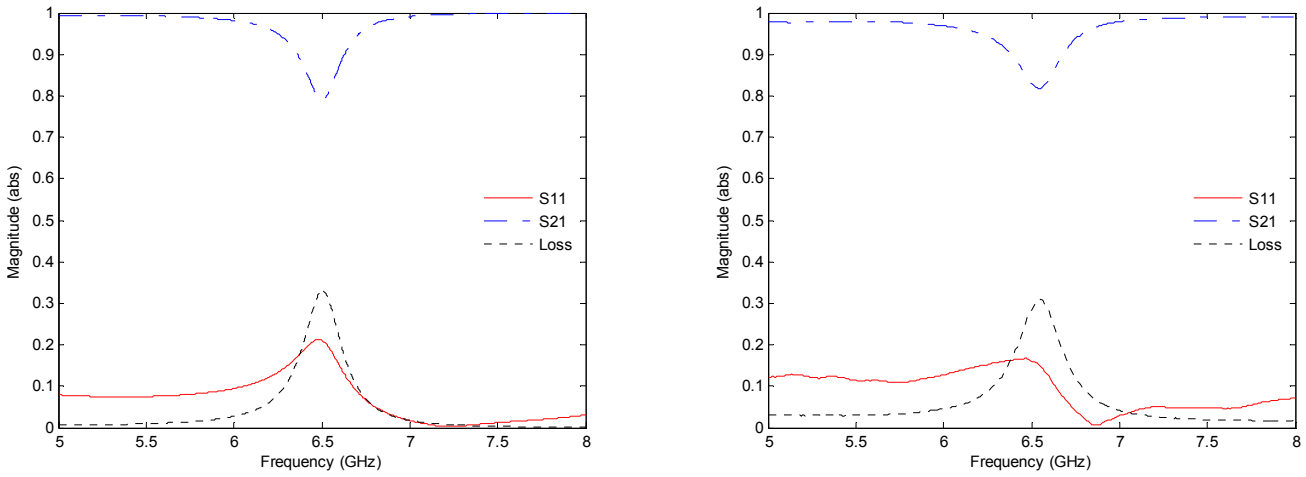

Figure 2.2: (a) Simulated and (b) measured S-parameters for the SRR loaded 0.35 λ_0 slot in a WR-137 waveguide.

Excellent agreement was obtained between the measured and simulated S-parameters. However, since the peak radiation direction is not at broad side (because of the offset position of the slot), it was necessary to measure the realised gain versus azimuth. The direction of peak radiation was then determined. This measurement was performed with a Waveline Inc. absorbing termination at Port 2 and may therefore be regarded as the unit cell case with travelling wave excitation. The measured realised gain in the peak radiation direction for the SRR loaded 0.35 λ_0 slot are compared with the unloaded 0.35 λ_0 slot and conventional (0.495 λ_0) slot in Figure 2.3.

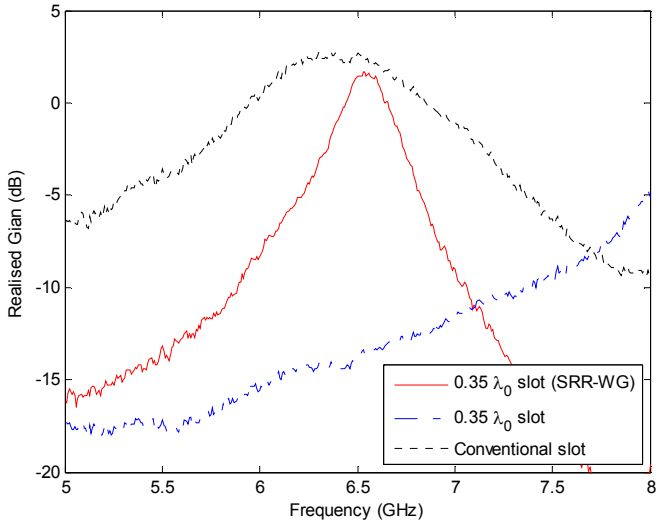

Figure 2.3: Measured peak realised gain for a single 0.35 λ_0 slot in a WR-137 waveguide with and without SRR loading compared to a conventional 0.495 λ_0 slot.

The SRR loaded 0.35 λ_0 slot achieved more than 15 dB enhancement over the unloaded 0.35 λ_0 slot at the design frequency of 6.5 GHz. Furthermore, the SRR loaded slot almost recovered the gain of the conventional (0.495 λ_0) slot at 6.5 GHz as expected. The small discrepancy between the two cases is attributed to the Ohmic and dielectric loss inherent to the SRR element. However, although great care was taken to ensure the correct position of the SRR element, there may be some inherent error attributed to the misplacement of the element beneath the slot.

The reduced bandwidth of the SRR-loaded slot (compared to a conventional resonant slot) is inconsequential for the SWASS concept since a conventional SWA array is analogous to a one-dimensional high-Q resonant structure with a typical bandwidth of only a few percent. However, for the SWASS concept, this reduction in slot length ensures greater separation between successive slot ends in the array and therefore represents a clear structural benefit over the conventional resonant slot design. The results from this section have been reported in [3]

For completeness, a simple four slot array (with 0.35 λ_0 length slots) was measured with and without the SRR elements and compared with the conventional (with 0.495 λ_0 length slots) SWA. The SRR dimensions are summarised in Table 2.1. The WR-137 test fixture with SRR elements installed is illustrated in Figure 2.5.

Figure 2.4: WR-137 test fixture (cover plate removed) with SRR elements arranged for the SWA array.

The Agilent PNA-X series vector network analyser was first calibrated against a A.R.A DRG-118/A horn antenna with known radiation performance. The SWA array was then installed in the range with a Waveline Inc. sliding short tuned to ensure the standing wave nodes coincide with the slot centres. The measured realised gain at 6.5 GHz is illustrated in Figure 2.5.

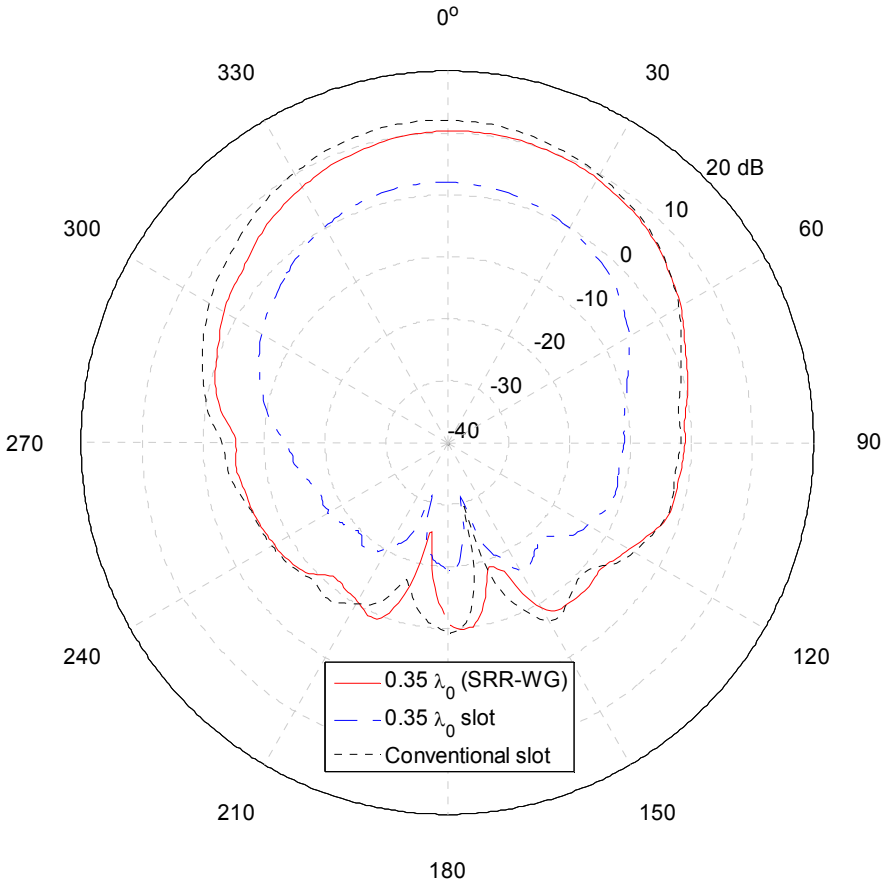

Figure 2.5: Measured realised gain in the y-x plane for the four slot SWA at 6.5 GHz. The 0.35 λ_0 slot in a WR-137 waveguide with and without SRR loading are compared to the conventional (0.495 λ_0) slot.

As expected, the SRR loaded slot array almost recovered the realised gain and pattern of the conventional resonant slot array. Note that the main lobe is symmetric in the y-x plane suggesting that equal power is radiated from each slot. This was also confirmed for the y-z plane in CST as illustrated in
Figure 2.6.

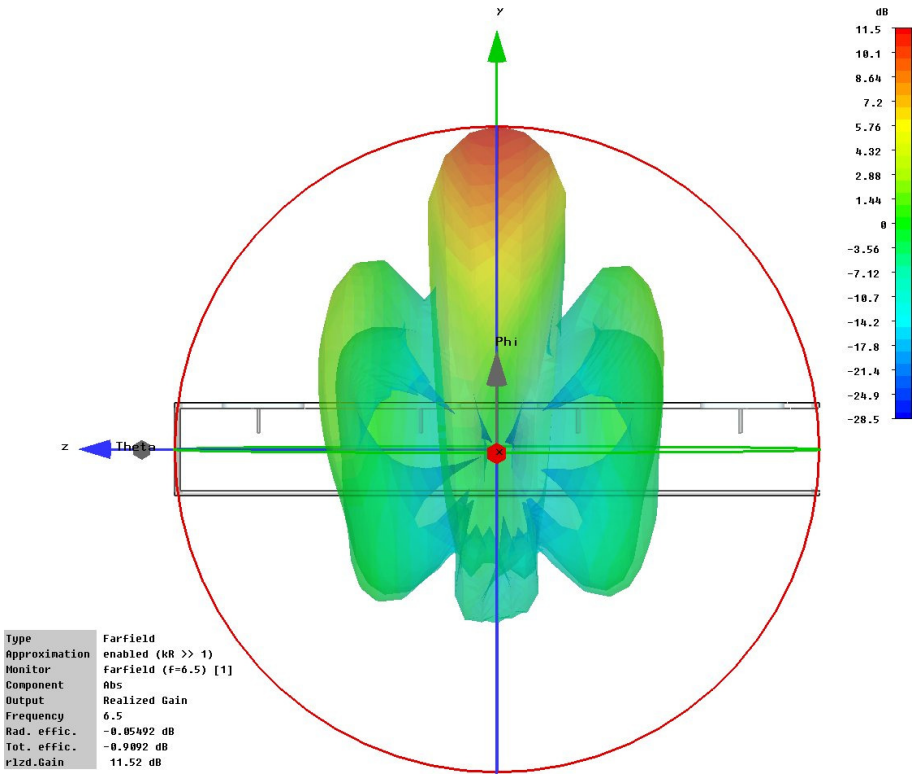

Figure 2.6: Simulated realised gain in the y-z plane for the four slot SWA with SRR loading at 6.5 GHz.

The simulated antenna pattern is symmetric in the y-z plane confirming that the SRR loaded SWA exhibits qualitatively similar radiation performance as the conventional SWA albeit with significantly reduced slot dimensions. Furthermore, the simulated peak realised gain compares favourably with the measured peak gain in Figure 2.5. The results from this section have been reported in [4].

3 BST Varactor Fabrication

Initially, the BST (Barium Strontium Titanate) films were deposited using the sputterer in RMIT University. The sputtering conditions were set to process gas of 100% Argon, gas pressure of 5 mTorr, deposition temperature of 700°C, RF power of 200 W and deposition time of eight hours. BST films of 400 nm thickness were obtained when characterised using profilometer and Scanning Electron Microscope (SEM) as captured in Figure 3.1. Further characterisation was done using X-Ray Diffraction (XRD) to characterise the crystal structure of the BST films.

As shown in Figure 3.2, the BST peaks corresponded to different crystallographic planes of (100), (110) and (111) in the XRD patterns and this can be concluded that the BST films were polycrystalline. Stronger (110) BST peaks were observed in all samples (BST 1, BST 2 and BST 3) than other peaks in the diffraction patterns. It is expected that by post-annealing a new batch of BST samples with the same sputtering conditions as mentioned in the coming weeks, the (111) BST peaks will become more intense and will be highly <111> oriented.

The varactors with different dimensions (including the gap between the fingers, the length of the capacitors and width of fingers) were fabricated on BST films on c-plane sapphire substrates in a multi-step process shown schematically in Figure 3.3. AZ1512 photoresist of

~1.2 µm thickness was spin coated onto the BST/sapphire sample in **A** and UV exposure was performed using MJB3 as shown in **B**. The sample was developed in AZ400K 1:4

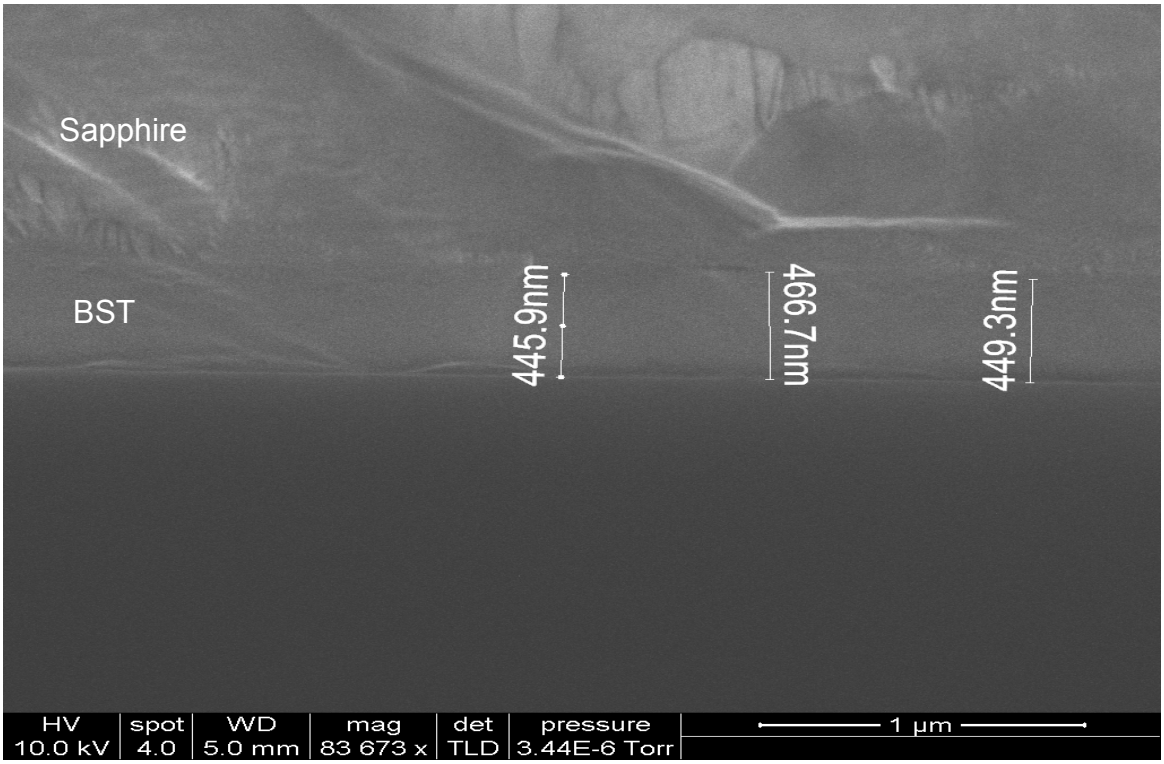

Figure 3.1: SEM images of a ~400 nm thick BST film on sapphire.

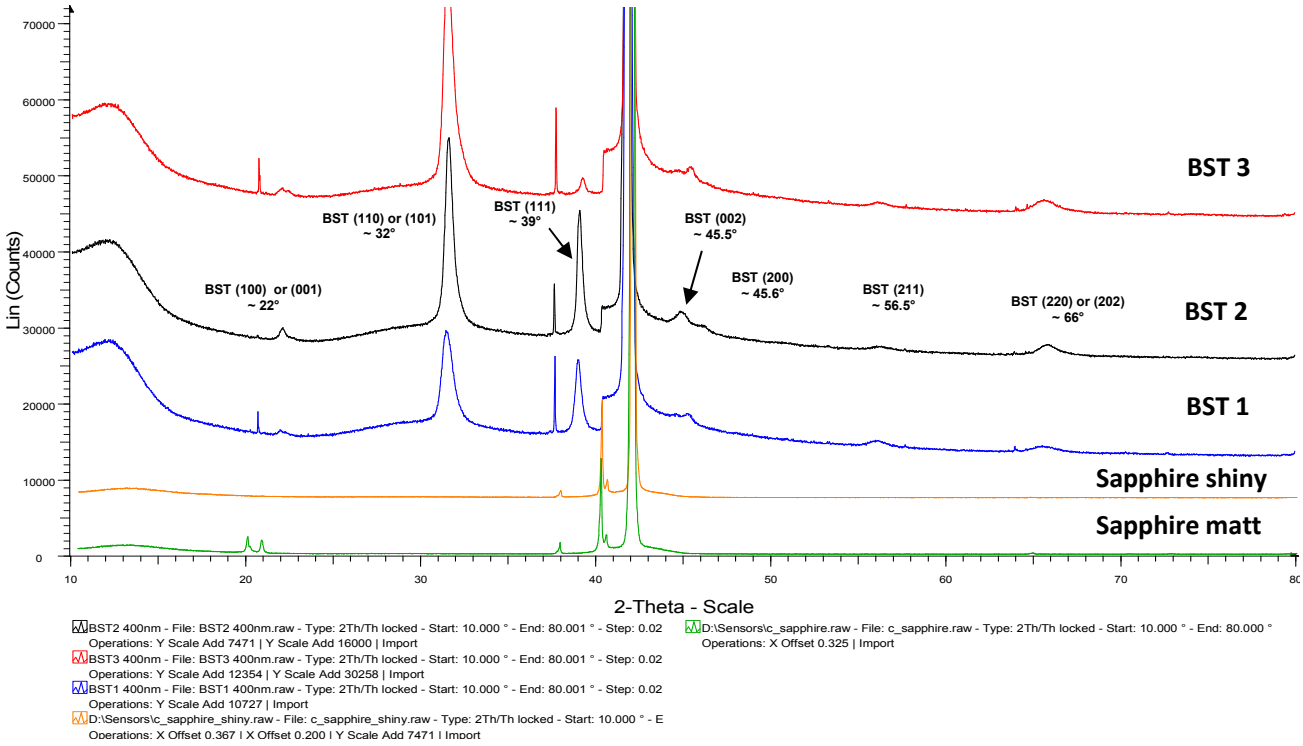

Figure 3.2: XRD patterns of BST thin films deposited on c-plane sapphire substrates.

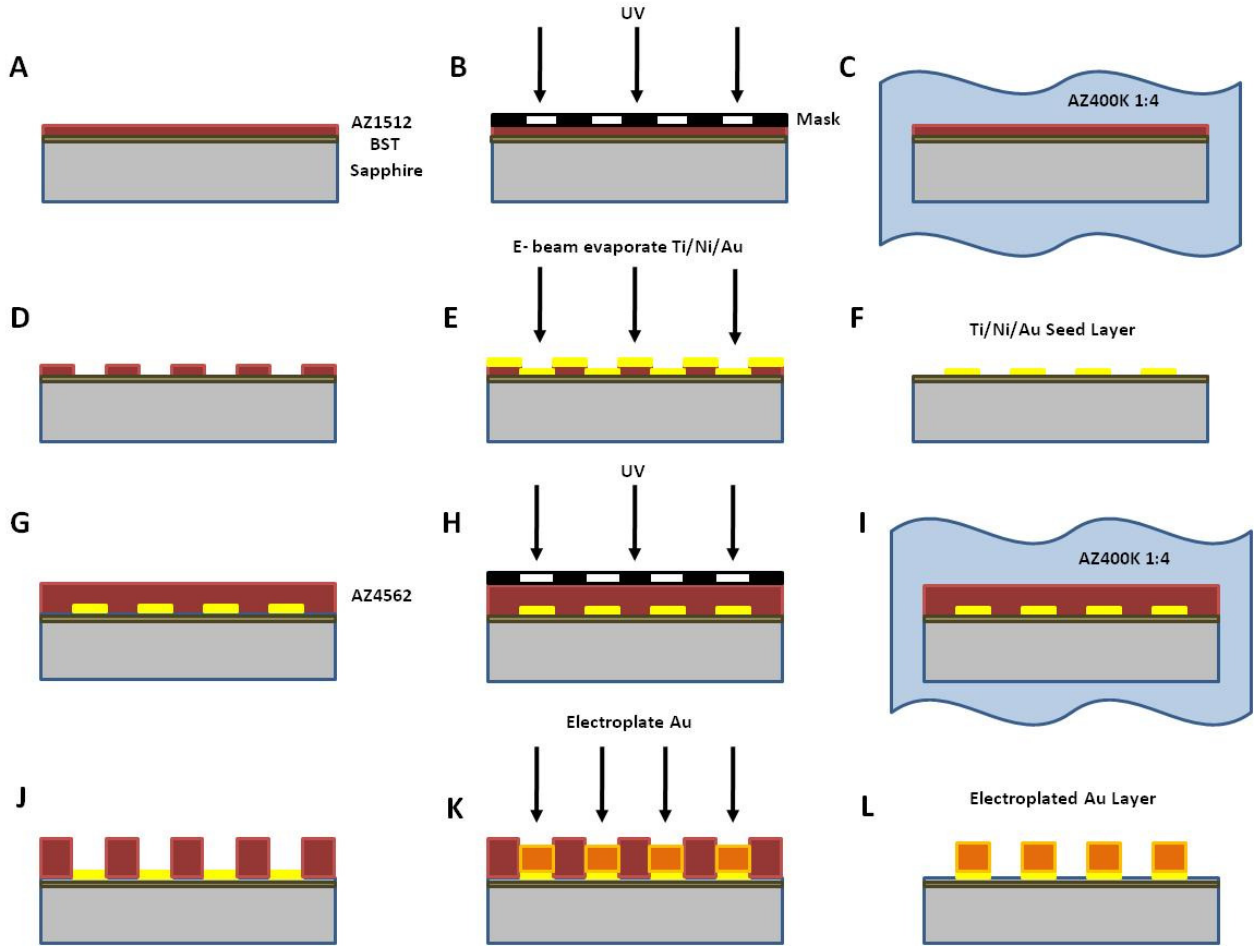

Figure 3.3: Fabrication process of BST varactors.

solution to define the area for depositing metals of seed layer for electroplating the BST varactor as depicted in **C** and **D** respectively. Layers of Ti/Ni/Au metals were deposited using an e-beam evaporator and the seed layer pattern was formed by liftoff as shown in **E** and **F** respectively. In **G, H, I** and **J**, AZ4562 photoresist of ~4 µm thickness was spin coated on the seed layer pattern and then was exposed and developed to define the region for electroplating Au. Au of approximately 3 µm thickness was electroplated on the seed layer and the sample was then rinsed with acetone, IPA and DI water to remove the unwanted resist in **K** and **L** respectively. The final product of BST varactors are shown in Figure 3.4.

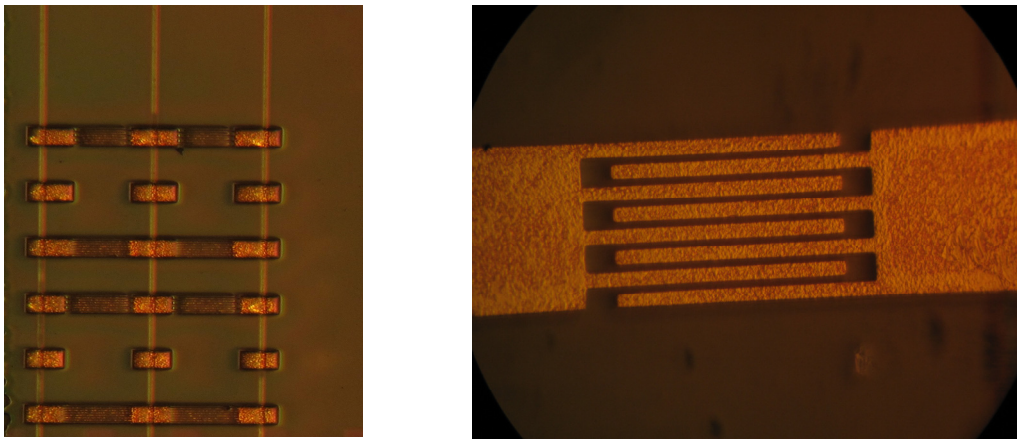

(a) (b)

Figure 3.4: (a) An array of BST varactors, and (b) a BST varactor with 2 μm finger gap, fixed 5 μm finger width and 130 μm finger length.

The BST varactors were measured on an Anritsu 37369A VNA connected to a wafer probe station. Calibration was initially performed using a CS-5 calibration substrate according to the standard SOLT calibration techniques. Microwave S-parameters of the BST varactors were then obtained by landing one GSG probe on the varactor measuring S_{11} parameters. DC bias voltage was externally supplied via the internal bias tee on the VNA which has limitation up to ±40 V.

An algorithm for fitting the equivalent circuit component values to measured S_{11} data was implemented in MATLAB and the capacitance values within frequency range of 1 to 20 GHz with biased voltage from 0 to 40 V were extracted. These extracted BST varactor capacitance values ranging from 0.75 to 0.92 pf at 0 and 40 V bias voltage is presented in Figure 3.5. This BST varactor with dimension of 2 μm finger gap, 130 μm length and fixed 5 μm finger width (for all varactors) produced the highest tunability of ~18% at 10 GHz. This result is very good compared to the previous work [5] for the un-annealed BST samples. It is expected in the coming weeks that by post-annealing a new batch of BST samples, the tunability will significantly improved due to the highly <111> oriented BST films. The simulated and measured nonlinear C-V characteristics of the BST varactor at 10 GHz are shown Figure 3.6.

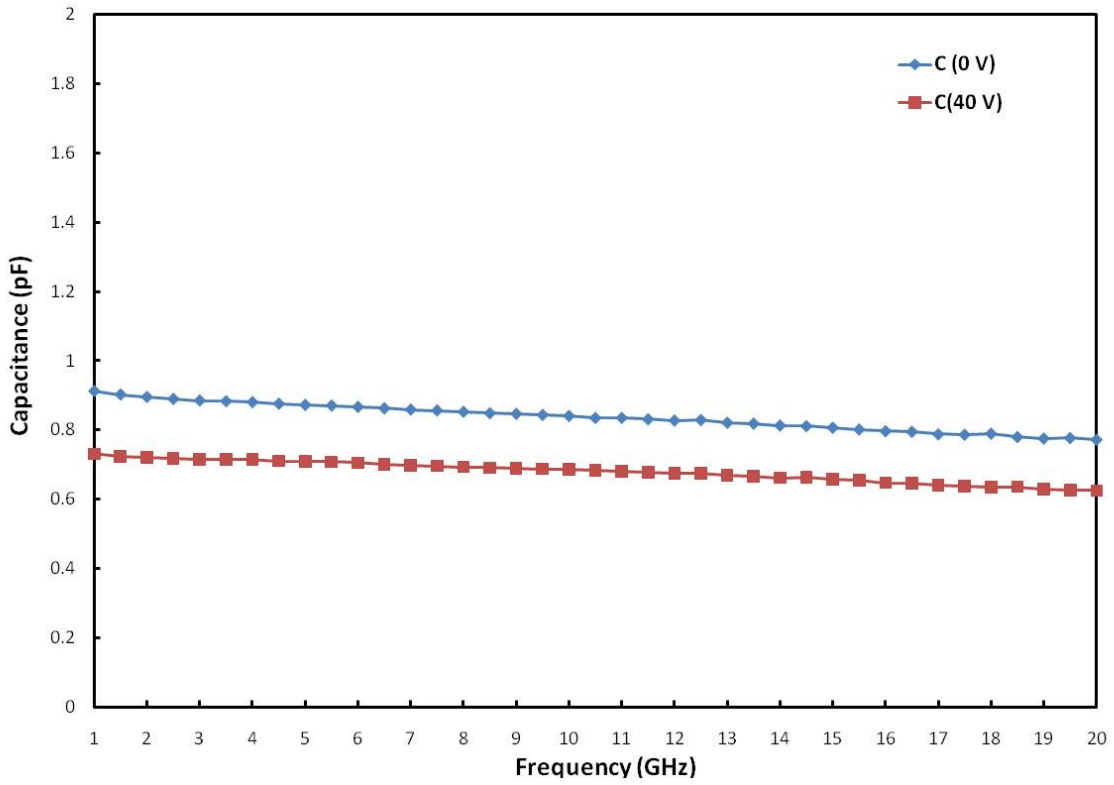

Figure 3.5: Extracted BST varactor capacitance values from 1 to 20 GHz at 0 and 40 V bias voltage with dimensions of 2 µm finger gap, fixed 5 µm finger width and 130 µm finger length.

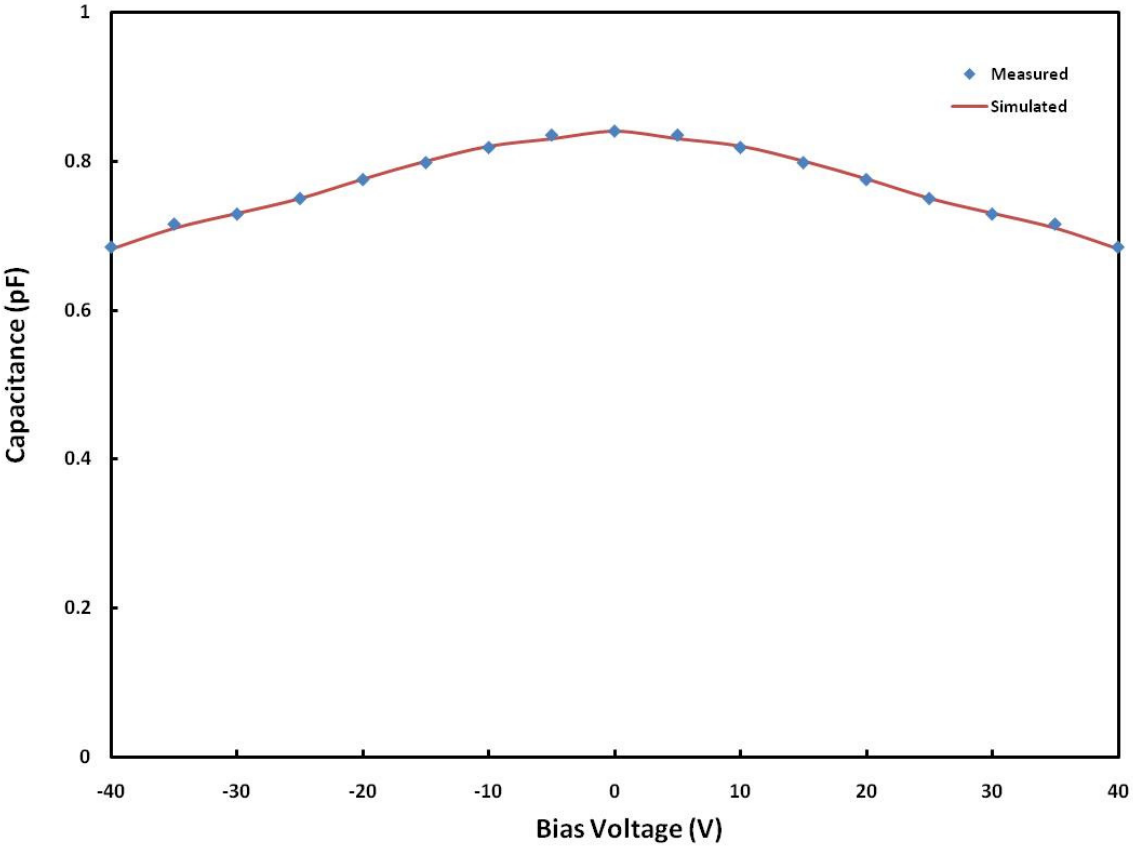

Figure 3.6: Simulated and measured C-V curves of the BST varactor at 10 GHz

4 Conclusions

This report validated a simple means to achieve acceptable gain from a miniaturized slot by utilising the strong fields induced in a SRR. If the added complexity of the SRR element and a small reduction in the peak gain can be tolerated, then further reduction of the slot length may also be possible. The presented method has therefore opened a new design space where the structural performance of the SWA is traded against the realized gain of the slot to achieve a truly multifunctional aircraft structure.

The development of BST varactors at RMIT has shown promising results in terms of its tunability and operating frequency. These varactors can operate at frequency range of 1 to 20 GHz with minimum variation. It is expected that the tunability can be significantly improved when post-annealing is added in the fabrication process.

5 References

[1] P. J. Callus, “Novel concepts for conformal load-bearing antenna structure,” DSTO, Technical Report DSTO-TR-2096, 2008.

[2] J. Sabat, “Structural response of slotted waveguide antenna stiffened structure components under compression,” AFIT, Technical Report AFIT/GAE/ENY/10-M19, 2010.

[3] K. J. Nicholson, W. S. T. Rowe, P. J. Callus, and K. Ghorbani, “Split-Ring Resonator Loading for the Slotted Waveguide Antenna Stiffened Structure,” *IEEE Antennas and Wireless Propagation Letters*, vol. 10, pp. 1524–1527, 2011.

[4] K. J. Nicholson, W. S. T. Rowe, P. J. Callus, and K. Ghorbani, “Split-ring Resonator Loaded Slot Array,” in *Asia Pacific Microwave Conference Proceedings*, Australia, 2011, pp. 1338–1341.

[5] E. A. Fardin, A. S. Holland, and K. Ghorbani, “Enhanced tunability of magnetron sputtered $Ba_{0.5}Sr_{0.5}TiO_3$ thin films on c-plane sapphire substrates,” Appl. Phys. Lett., vol. 89, no. 2, pp. 022901, July 2006.